PERGAMON

International Journal of Heat and Mass Transfer 44 (2001) 3799–3810

International Journal of HEAT and MASS TRANSFER

www.elsevier.com/locate/ijhmt

Fully developed turbulent flow and heat transfer at fiber-flocked surfaces

Kurt O. Lund *

Center for Energy Research, Department of Mechanical and Aerospace Engineering, Jacobs School of Engineering, University of California, La Jolla, CA 92093-0417, USA

Received 20 October 1999; received in revised form 9 January 2001

Abstract

High-conductivity carbon fibers can be "flocked", or perpendicularly attached onto surfaces, thus enabling heat transfer enhancement for such fiber-flocked surfaces. An analysis is performed for fully developed turbulent flow and heat transfer in ducts with high-conductivity fibers covering the walls. The fiber volumetric packing density is sparse such that single-cylinder correlations are used for the fiber drag and Nusselt number; this gives rise to body-type terms in the momentum and energy equations for the region near the wall covered with fibers.

An eddy-diffusivity type turbulence model is employed, including Laufer core-flow distribution and Van Driest damping, but with a shifted origin. The resulting core- and fiber-region equations are solved by the singular perturbation theory, and matched at the fiber-tip interface, yielding a friction factor function that is fitted to available experimental data with a 32% fiber-length coordinate shift.

The results show the variation of the duct Nusselt number with Reynolds number to be similar to that for smooth surfaces, but with an enhancement factor of *four* for gases. A very strong variation with Prandtl number is predicted for the fiber-flocked surfaces; for liquid metals and gases a moderate enhancement is predicted, whereas for water and viscous liquids an order-of-magnitude enhancement appears possible.

1. Introduction

The present work is an outgrowth of the previous analysis that considered fiber-enhanced heat transfer under *laminar* flow conditions [1]; in that work, it was shown that the placement of high-conductivity fibers in the wall region reduces the wall thermal resistance, thus enhancing the heat transfer at the fiber-covered surface. This effect is expected to be even more pronounced in *turbulent* flow because of the steep velocity and temperature gradients near the wall. Therefore, we here consider the fully developed turbulent flow and heat transfer in ducts having surfaces sparsely covered with filaments or fibers, and for filaments which are short compared to the overall duct diameter or width. High-conductivity carbon-fiber filaments are typically *flocked* onto the surface, but can be limited to the wall region of the shear flow.

Other, previous investigations of flow and heat transfer at fiber-covered surfaces are for the application to mammals covered with hair [2,3]; in these studies, the hair filaments were comparatively long with dense packing, so that porous-media flow was used as a modeling basis, including uniform flow throughout the medium [2]. These models for determining the insulating effects of hair are not applicable to the present sparse-packing conditions for enhanced heat transfer; instead, we consider single-filament correlations to apply to the flow and temperature fields between the filaments.

Owing to the sparse packing, turbulent fluctuations will penetrate the fiber region to some extent, but the degree cannot be predicted by any available turbulence theories. Therefore, the turbulent flow and temperature fields are here modeled in terms of the elementary eddy-diffusivity theory, including shifted profiles that are traditionally used with sand-roughened surfaces [4–6];

* Tel.: +1-858-481-8914; fax: +1-858-793-2446.
E-mail address: klund@electriciti.com (K.O. Lund).

0017-9310/01/$ - see front matter
PII: S0017-9310(01)00045-X

Nomenclature

A	cross-sectional area
B_0	friction law parameter
C_0	friction law parameter
C_D	fiber drag coefficient
D_H	duct hydraulic diameter
d	fiber diameter
d^+	scaled fiber diameter, $U_\tau d/\nu$
F	core outer velocity function
f	core inner velocity function
f	Darcy friction factor
f_D	volumetric fiber drag force, $2\sigma\rho U^2 C_D/(\pi d)$
G	core temperature function
g	fiber drag function
H	fiber length (height above wall)
h	fiber-surface heat transfer coefficient
h	nondimensional fiber length, H/R_H
h^+	scaled fiber length, HU_τ/ν
I_m	integral function (4c)
J_m	constant, $J_m = I_m(\infty)$
k	thermal conductivity
M	Laufer diffusivity function (1d)
N	Van Driest diffusivity function (1d)
Nu	duct hydraulic-diameter Nusselt number
Nu_d	fiber-diameter Nusselt number, hd/k_g
n	duct shape index ($=0$ for plane, $=1$ for circular)
n	exponent in drag correlation
P	perimeter, polynomial eddy-diffusivity function (1e)
Pr	Prandtl number
Pr_t	turbulent Prandtl number
p	pressure, ratio of Prandtl numbers, Pr/Pr_t
Q_m	integral function (3c)
q	heat flux
R	radial distance from centerline
R_H	radial distance to fiber tips
R^+	friction Reynolds number, $R_H U_\tau/\nu$
Re	duct Reynolds number, $U_m D_H/\nu$
Re_d	fiber Reynolds number, Ud/ν
r_h	ratio, $(1+\gamma)/(1+0.4\gamma)$
r_k	ratio, $k_s\sigma/k_g(1-\sigma)$
S	heat source parameter
s	friction parameter, $U_\tau/\kappa V_C$
T	temperature
U	axial velocity
U_H	axial velocity at $Y = H$
U_m	duct mean velocity
U_τ	shear velocity at $Y = H$, $\sqrt{(\tau_H/\rho)}$
u^+	nondimensional axial velocity, U/U_τ
u_h^+	nondimensional axial velocity, U_H/U_τ
u_m^+	nondimensional duct-average axial velocity, U_m/U_τ
V	shifted axial velocity
V_C	shifted axial velocity on centerline
v	nondimensional shifted velocity, V/V_C
W	turbulent diffusivity coordinate, $Y - Y_t$
w	nondimensional diffusivity coordinate, $W/R_H = z + \lambda$
X	axial coordinate
Y	transverse coordinate (distance from wall)
Y_t	eddy-diffusivity shift from wall
y	nondimensional coordinate, Y/R_H
y_t	eddy-diffusivity shift from wall, Y_t/R_H
Z	shifted transverse coordinate, $Y - H$
z	nondimensional shifted coordinate, Z/R_H

Greek symbols

α	thermal molecular diffusivity
δ	fiber slenderness ratio, d/H
ε	flow perturbation parameter
ε_H	heat transfer perturbation parameter
ϕ	ratio of mean to centerline velocity
Γ	thermal diffusivity ratio, $1 + pv_t/\nu$
γ	drag parameter, $\gamma = 0.4(d^+ u_h^+)^{3/4}$
η	fiber-region inner coordinate, $(h-y)/\varepsilon$
η_H	fiber-region inner coordinate, $(h-y)/\varepsilon_H$
θ	scaled temperature, $(T - T_w)/(T_H - T_w)$
κ	von Karman constant, 0.41
Λ	parameter in (7d) and (8)
λ	turbulence shift distance, $h - y_t$
μ	viscosity
ν	molecular momentum diffusivity
ν_t	turbulent momentum diffusivity
ψ	scaled temperature, θ/S
ρ	fluid density
σ	solid (fiber-region) volumetric packing fraction
τ	total shear stress
ξ	friction Reynolds parameter, $\kappa R_H U_\tau/\nu = \kappa R^+$
ζ	core inner, stretched coordinate, $\xi(z+\lambda)$
Ω	heat transfer constant, $\sqrt{(1 + r_k/\Gamma)}$
ω	flow constant, $1/\omega^2 = 1/\xi + M(\lambda)N(\xi\lambda)$

Subscripts and superscripts

C, c	core region
CL	centerline
d	fiber diameter
g	fluid (gas)
H	valuation at $Y = H$, heat transfer
h	valuation at $y = h$
i	inner asymptotic region
m	core bulk average, integral index
o	outer asymptotic region
s	solid (fiber)
t	turbulent
w	wall
+	wall-region variable

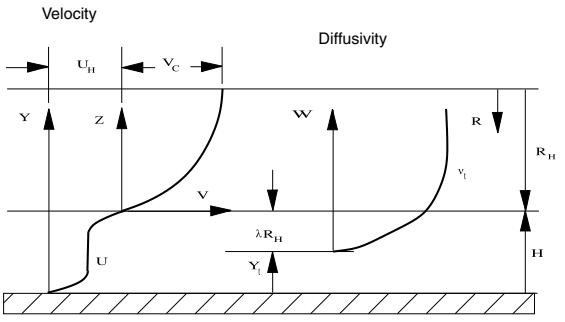

Fig. 1. Problem definition diagram.

recent studies with other types of roughness confirm the validity of shifted profiles [7–9].

As in previous asymptotic analyses of turbulent flows [10,11], the shear stress and the velocity gradient are related by the sum of the molecular and turbulent diffusivities: $\tau = \rho(\nu + \nu_t)\mathrm{d}U/\mathrm{d}Y$; however, the turbulent diffusivity is here taken to dampen out at virtual origin $Y = Y_t$ (instead of $Y = 0$ for smooth walls), where Y_t is determined from experiment. Therefore, in similarity to previous work [10,11], we take $\nu_t = \nu \times M(w)N(w^+)$, where the diffusivity coordinate is $w = y - y_t = z + \lambda$, as shown in Fig. 1, $w^+ = WU_\tau/\nu$, and where M and N are the functions to be defined.

The previous analysis for laminar flow [1] showed that the fiber drag was much greater than the wall shear at $Y = 0$, and that the largest shear tended to occur near the fiber tips at $Y = H$. We therefore take the turbulence to scale with this maximum shear (instead of the wall shear) and define the friction velocity as $U_\tau \equiv \sqrt{(\tau_H/\rho)}$, where τ_H is the shear stress at $Y = H$.

Energy transport in the fiber region consists of conduction in the fibers and convection between the fibers. The turbulent diffusivity of heat is taken proportional to ν_t through a constant turbulent Prandtl number [6].

With these models, the momentum and energy equations are stated for the turbulent core and the fiber regions, and the respective solutions are matched at the interface, as previously [1]. For a constant wall heat flux, the results show a significant increase in the Nusselt number compared to other surface augmentation techniques.

2. Flow analysis

2.1. Derivation of momentum equations

For the turbulent flow analysis, the velocity is divided into the core region and the fiber region, as shown in Fig. 1. Here the core velocity, $U(R)$, is defined in terms of the shifted coordinate system,

$$U = U_H + V(Z),$$

where $Z = Y - H$, and U_H is the interface velocity at the tips of the fibers, as indicated; thus, $V(0) = 0$ at $Y = H$ ($R = R_H$), and $V = V_C$ at $Z = R_H$ ($R = 0$). Here R is the radial distance from the center of a circular duct, or the distance from the centerline for a planar duct.

2.1.1. Core-region momentum equation

A force balance on a differential element in the core of a round pipe yields the equation for the total (laminar + turbulent)shear stress, τ:

$$\frac{1}{R^n}\frac{\partial(R^n\tau)}{\partial R} = -\frac{\partial p}{\partial X} = \text{const.} \tag{1a}$$

For the turbulent core where there are no fibers, (1a) has the first integral $\tau = \tau_H(R/R_H)$; thus, in terms of $Z = R_H - R$, the core stress is

$$\tau = \tau_H(1 - Z/R_H) = \tau_H(1 - z) = \rho U_\tau^2(1 - z).$$

Let τ be related to the velocity gradient by the total viscosity:

$$\tau = \rho(\nu + \nu_t)\frac{\mathrm{d}V}{\mathrm{d}Z}.$$

Then the core momentum equation for both circular and planar ducts is

$$\nu\left(1 + \frac{\nu_t}{\nu}\right)\frac{\mathrm{d}V}{\mathrm{d}Z} = \frac{\nu V_c}{R_H}\left(1 + \frac{\nu_t}{\nu}\right)\frac{\mathrm{d}v}{\mathrm{d}z} = U_\tau^2(1 - z). \tag{1b}$$

Except for boundary conditions at the tips of the fibers ($z = 0$), (1b) is identical to conventional turbulent duct flow, but with ν_t "disappearing" below 0 at $z = -\lambda$, as typical for rough-surface flows [4–6], and as indicated in Fig. 1; therefore, (1b) can be written as the singular perturbation problem [10,11]:

$$\left(\frac{1}{\xi} + M[z + \lambda]N[\xi(z + \lambda)]\right)\frac{\mathrm{d}v}{\mathrm{d}z} = s(1 - z), \tag{1c}$$

where the Laufer (M)and Van Driest (N) eddy-diffusivity functions are [10,11]:

$$M(y) = \frac{y}{1 + yP(y)}, \quad N(\zeta) = \left[1 - \mathrm{e}^{-\zeta/6.9}\right]^2. \tag{1d}$$

Based on the data of Laufer for circular ducts [12], and on the data of Hussain and Reynolds for plane ducts [13], the function $P(y)$ is represented as the polynomials

$$P(y) \approx \begin{cases} 0.62(1 + 11.8y - 4.6y^2), & \text{circular} \\ 0.44(1 + 13.8y - 2.9y^2), & \text{planar} \end{cases} \tag{1e}$$

with the resulting eddy diffusivities shown in Fig. 2. Because ξ is large, N decays to zero a short distance above the fibers; however, N is essential immediately near and between the fiber tips.

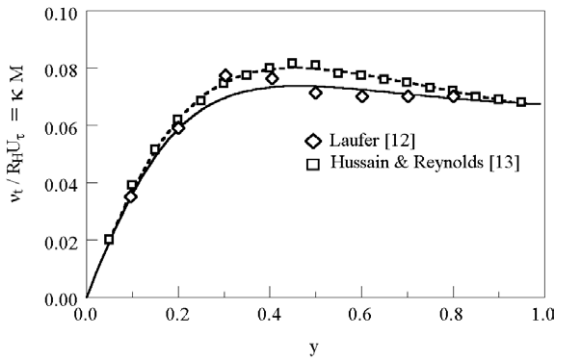

Fig. 2. Eddy diffusivity.

2.1.2. Fiber-region momentum equation

Consider a surface flocked with fibers of length H and diameter d. Because the fibers are short relative to the duct radius, the curvature effect in this region near the wall is negligible. Thus, a force balance on a differential element at distance Y yields the following [1]:

$$(1-\sigma)\frac{\partial \tau}{\partial Y} - f_D = -\left(-\frac{\partial p}{\partial X}\right) \equiv -\frac{\rho U_\tau^2}{R_H}. \tag{2a}$$

Therefore, with $\tau = \rho(\nu + \nu_t)\partial U/\partial Y$, the fiber-region momentum equation is

$$(1-\sigma)\frac{\partial}{\partial Y}\left[(\nu+\nu_t)\frac{\partial U}{\partial Y}\right] - \frac{2\sigma}{\pi d}U^2 C_D = -\frac{U_\tau^2}{R_H}. \tag{2b}$$

Let $u^+ = U/U_\tau$ and $y = Y/R_H$. Then the nondimensional equation results

$$\frac{1-\sigma}{R^+}\frac{\partial}{\partial y}\left[(1+\nu_t/\nu)\frac{\partial u^+}{\partial y}\right] - \frac{2\sigma R^+}{\pi d^+}u^{+2}C_D = -1. \tag{2c}$$

A correlation of drag coefficients for single circular cylinders in cross-flow was developed previously, which is valid over a large Reynolds number range [1]:

$$C_D = 1 + \frac{10}{Re_d^n} = \frac{10}{Re_d^n}\left(1 + \frac{Re_d^n}{10}\right) = \frac{10}{d^{+n}}\left(\frac{1}{u^{+n}} + \frac{d^{+n}}{10}\right), \tag{2d}$$

where $Re_d = u^+ d^+$ and $n = 3/4$. Substitution of (2d) into (2c) then yields the fiber-region momentum equation

$$\frac{1-\sigma}{R^+}\frac{\partial}{\partial y}\left[(1+\nu_t/\nu)\frac{\partial u^+}{\partial y}\right] - \frac{20\sigma R^+}{\pi (d^+)^{7/4}}g(u^+) = -1, \tag{2e}$$

where $g(u^+) = (u^+)^{5/4} + 0.1(d^+)^{3/4}(u^+)^2$. For the analytical solution of (2e) it is convenient to expand the fiber drag term in a Taylor Series about u_h^+:

$$g(u^+) \approx g(u_h^+) + (u^+ - u_h^+)g'(u_h^+) = \frac{5}{4}(u_h^+)^{1/4}(1+0.4\gamma)\left(u^+ - \frac{u_h^+}{5}\frac{1+\gamma}{1+0.4\gamma}\right),$$

where $\gamma = 0.4(d^+u_h^+)^{3/4}$; then, (2e) is written as

$$\varepsilon^2\frac{\mathrm{d}}{\mathrm{d}y}\left[\left(\frac{1}{\xi} + M[y-y_t]N[\xi(y-y_t)]\right)\frac{\mathrm{d}u^+}{\mathrm{d}y}\right] - u^+ = -\frac{u_h^+}{5}r_h + \cdots, \tag{2f}$$

where

$$r_h = \frac{1+\gamma}{1+0.4\gamma} = \frac{1+0.40(d^+u_h^+)^{3/4}}{1+0.16(d^+u_h^+)^{3/4}},$$

and the leading multiplier is considered a small number

$$\varepsilon \equiv \sqrt{\frac{\pi(1-\sigma)(d^+)^{7/4}}{25\sigma R^+(u_h^+)^{1/4}(1+0.4\gamma)}} = \frac{d^+}{5}\sqrt{\frac{\pi(1-\sigma)}{\sigma R^+(d^+u_h^+)^{1/4}(1+0.4\gamma)}} \prec\prec 1. \tag{2g}$$

That is, we limit the investigation to very small slenderness ratios, $d^+ = \delta h^+$ (e.g., $\delta < 0.01$), and large R^+ so that $\varepsilon \ll 1$. With small ε, (2f) constitutes a *double* singular perturbation problem which can be solved for $\varepsilon \to 0$ and $\xi \to \infty$ as previously for smooth wall-bounded shear flows [10,11]. However, for small ε, we shall find that both laminar and turbulent layers can be included together in the fiber region such that the limit, $\xi \to \infty$, is not needed to match these layers.

2.2. Solution of momentum equations

The core- and fiber-region equations (1c) and (2f), are both singular perturbation equations for $\xi \to \infty$ (large Reynolds number); that is, we seek solutions for negligible molecular viscosity relative to turbulent viscosity. This will be true in most of the core region (*core outer region*), but close to the fibers both terms are of equal importance (*core inner region*); therefore, for the latter, an *inner* stretched coordinate is defined, $\zeta = \xi(z+\lambda)$. For the fibers, the *outer fiber region* is near the center of the fiber lengths, and the *inner fiber region* is near the tips of the fibers; thus, the *inner* stretched coordinate here is $\eta = (h-y)/\varepsilon$. The inner and outer solutions are joined by matched asymptotic expansions, and these matched solutions furthermore have matched values and slopes at the fiber tips ($y = h$).

2.2.1. Core-region solution

For the *outer* core region let $v = 1 + sF(w;\xi) = 1 + s\{F_0(w) + F_1(w)/\xi + \cdots\}$. Then to lowest order, (1c) is:

$$(M[w])\frac{\mathrm{d}F_0}{\mathrm{d}w} = 1 + \lambda - w, \qquad \frac{\mathrm{d}F_0}{\mathrm{d}w} = \left(\frac{1}{w} + P(w)\right)(1+\lambda-w). \tag{3a}$$

The solution of (3a), subject to $F(1+\lambda;\xi)=0$, is

$$F_0(w) = (1+\lambda)\ln\left(\frac{w}{1+\lambda}\right) + (1+\lambda-w)[1-Q_1(w)], \tag{3b}$$

where $Q_m(w)$ is the integral

$$Q_m(w) = \frac{1}{(1+\lambda-w)^m}\int_w^{1+\lambda}(1+\lambda-t)^m P(t)\,dt. \tag{3c}$$

Thus, the core-outer-region velocity is

$$v^o(z) = 1 + s(1+\lambda)\left\{\ln\left(\frac{z+\lambda}{1+\lambda}\right) + \frac{(1-z)[1-Q_1(z+\lambda)]}{1+\lambda}\right\}. \tag{3d}$$

For the core-region *inner* solution (near the fiber tips), we take $\zeta=\xi(z+\lambda)=\xi w$, and $v(z;\xi)=s[f(\zeta)-f(\xi\lambda)]$; then $v(0;\xi)=0$ and, to lowest order as $\xi\to\infty$, (1c) is

$$(1+\zeta N[\zeta])\frac{df_0}{d\zeta} = 1+\lambda. \tag{4a}$$

The solution of (4a) is similar to previous, smooth-wall results [10]:

$$f_0(\zeta) = (1+\lambda)[\ln(1+\zeta)+I_0(\zeta)], \tag{4b}$$

where I_m is the integral

$$I_m(\zeta) = \int_0^\zeta \frac{p^m t}{1+p^m t}\frac{1-N(t)}{1+p^m t N(t)}\,dt, \tag{4c}$$

thus, to lowest order, the core inner solution is

$$v^i(\zeta) = s(1+\lambda)\left[\ln\left(\frac{1+\zeta}{1+\xi\lambda}\right) + I_0(\zeta) - I_0(\xi\lambda)\right]. \tag{4d}$$

To match the core inner and outer solutions, the same function must be obtained in the limits of v^i as $\zeta\to\infty$,

$$v^i \to s(1+\lambda)\left[\ln(z+\lambda) + \ln\left(\frac{\xi}{1+\xi\lambda}\right) + J_0 - I_0(\xi\lambda)\right], \tag{4e}$$

and of v^o as $z\to 0$,

$$v^o \to 1 + s(1+\lambda)\left\{\ln(z+\lambda) + 1 - \ln(1+\lambda) - \frac{Q_1(\lambda)}{1+\lambda}\right\}. \tag{4f}$$

It is seen that these limits are the same function when

$$s(1+\lambda)\left[\ln\left(\frac{\xi}{1+\xi\lambda}\right) + J_0 - I_0(\xi\lambda)\right] = 1 + s(1+\lambda)\left\{1 - \ln(1+\lambda) - \frac{Q_1(\lambda)}{1+\lambda}\right\},$$

or

$$\frac{1}{s(1+\lambda)} = \ln\xi + B_0,$$
$$B_0 = J_0 + \frac{Q_1(\lambda)}{1+\lambda} - 1 - [I_0(\xi\lambda) + \ln(1+\xi\lambda)], \tag{5a}$$

since λ is of order $h \ll 1$, this result simplifies to

$$\frac{\kappa V_C}{U_\tau} \equiv \frac{1}{s} = \ln\xi + B_0,$$
$$B_0 = C_0 - [I_0(\xi\lambda) + \ln(1+\xi\lambda)], \tag{5b}$$

where $C_0 = J_0 + Q_1(0) - 1 \approx 3.26$. It is noted that for $\lambda\equiv 0, B_0 = C_0$; although λ is small, the product $\xi\lambda$ is not. Now, the overall core-flow distribution is only marginally affected by the short fibers; therefore, the ratio of shifted mean velocity to centerline velocity can be taken as the same for smooth ducts, $V_m/V_C = \phi$ ($\approx$0.82 for circular ducts [6] and $\approx$0.89 for plane ducts [13]); hence we obtain the mean velocity $U_m = U_H + \phi V_C$ and the expression for u_m^+:

$$\frac{1}{s} = \kappa\frac{u_m^+ - u_h^+}{\phi} = \ln\xi + B_0,$$

or

$$u_m^+ = u_h^+ + \frac{\phi}{\kappa}(\ln\xi + B_0(\xi\lambda)). \tag{5c}$$

With the above relationships for s, a uniformly valid core composite expansion is

$$(v^+)^c = \frac{1}{\kappa}[\ln(1+\zeta) + I_0(\zeta) - I_0(\xi\lambda) + (1-z)[1-Q_1(z+\lambda)]] \tag{5d}$$

with the absolute core velocity given by $u^+ = u_h^+ + v^{+c}$. This expression compares to the composite expansion for smooth walls:

$$(u_s^+)^c = \frac{1}{\kappa}[\ln(1+\xi y) + I_0(\xi y) + (1-y)[1-Q_1(y)]]. \tag{5e}$$

2.2.2. Fiber-region solution

The fiber-region *outer* solution of (2f) as $\varepsilon\to 0$ (for the fiber mid-section) is, simply, the constant velocity, $u^{+o} = u_h^+ r_h/5$. An *inner* solution exists at the top of the fibers with $\eta = (h-y)/\varepsilon$; however, the one at the bottom is neglected for this turbulent flow. The resulting *inner* equation is therefore

$$\frac{d}{d\eta}\left[\left(\frac{1}{\xi} + M[h-y_t-\varepsilon\eta]N[\xi(h-y_t-\varepsilon\eta)]\right)\frac{du^+}{d\eta}\right] - u^+ = -u^{+o} + \cdots, \tag{6a}$$

thus, to lowest order, as $\varepsilon \to 0$

$$\left(\frac{1}{\xi} + M[\lambda]N[\xi\lambda]\right)\frac{d^2u^+}{d\eta^2} - u^+ = -u^{+o} + \cdots. \tag{6b}$$

Because the limit $\varepsilon \to 0$ causes the turbulent diffusivity to become constant in η, both the laminar and turbulent parts are here treated together and the limit $\xi \to \infty$ is not required. Thus, the solution of (6b) to lowest order in ε is

$$\begin{aligned} u^+ &= \frac{u_h^+}{5}\{r_h + (5 - r_h)e^{-\omega\eta}\}, \\ \frac{1}{\omega^2} &= \frac{1}{\xi} + M[\lambda]N[\xi\lambda]. \end{aligned} \tag{6c}$$

The core distribution, (5d), and this solution are shown in Fig. 3 for the circular duct, and for $\lambda = 0.32h$ (for subsequent fitting to experiments), where the log–log scale emphasizes the fiber-region. The usual full turbulent velocity profile, but shifted and joined to the fiber-region flow at $h = 0.02$ (dashed line) is also shown. Both the values and slopes of the velocity profiles agree at the interface (as further discussed below) where the shear "pulls along" the fiber-region flow.

In conventional wall variables this curve is shown in Fig. 4, in comparison to the smooth profile (5e). It is seen that the velocity profile is shifted downwards as the fibers are approached, in comparison to the smooth-wall profile, whereas there is only a marginal effect in the core, as expected. This is an important behavior because it is the turbulent flow in the vicinity of the fiber tips that will effect heat transfer from the fibers, as shown previously [1]. For the case calculated in Fig. 4 the core velocity profile approaches the fiber-region at $h^+ = 3.4$, as seen; there is a significant "retardation" of the flow due to the fibers below h^+.

Now, from (6c), the gradient of the fiber-region velocity is

$$\frac{du^+}{dy} = \frac{u_h^+\omega}{5\varepsilon}(5 - r_h)e^{-\omega\eta} \to \frac{u_h^+\omega}{5\varepsilon}(5 - r_h) \quad \text{as } \eta \to 0. \tag{7a}$$

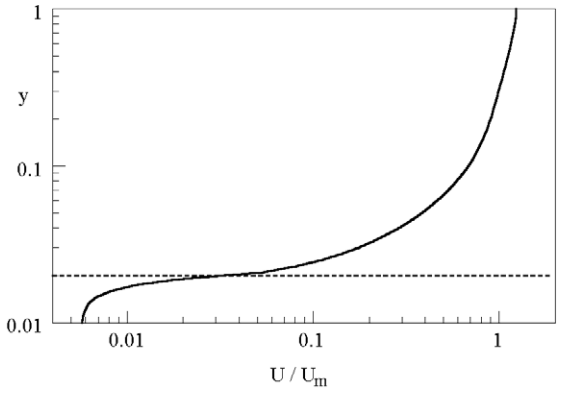

Fig. 3. Typical velocity profile.

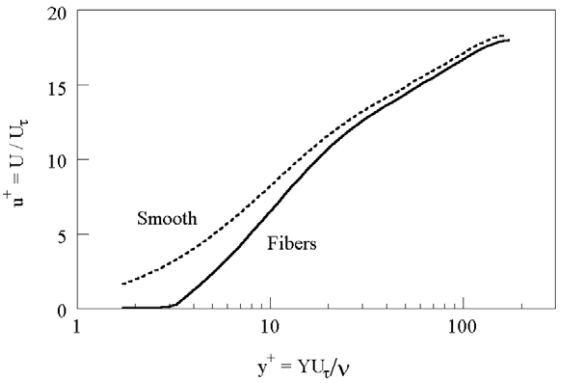

Fig. 4. Smooth- and fiber-surface velocity profiles.

That is, at the tip of the fibers the gradient or slope of the velocity profile becomes infinitely steep as $\varepsilon \to 0$, in order to meet $u^+ = u_h^+$ at $y = h$ ($\eta = 0$). Also, the gradient of the core-region velocity profile is obtained from (4a) as

$$\left.\frac{du^+}{dy}\right|_{y=h} = \frac{V_m}{\phi U_\tau}\left.\frac{dv}{dz}\right|_{z=0} = \frac{1}{\phi}\left(u_m^+ - u_h^+\right)\frac{\xi s}{1 + \xi\lambda N(\xi\lambda)}, \tag{7b}$$

and it is necessary that shear forces equate at the fiber-tip interface; therefore, comparing (7a) and (7b) we have

$$(1 - \sigma)\frac{u_h^+\omega}{5\varepsilon}(5 - r_h) = \frac{1}{\phi}\left(u_m^+ - u_h^+\right)\frac{\xi s}{1 + \xi\lambda N(\xi\lambda)}, \tag{7c}$$

or, to match shear forces, the interface velocity is obtained from

$$\begin{aligned} u_h^+ &= \frac{5\varepsilon}{\phi\omega(1 - \sigma)(5 - r_h)}\frac{\xi s}{1 + \xi\lambda N(\xi\lambda)}\left(u_m^+ - u_h^+\right) \\ &\equiv \Lambda\left(u_m^+ - u_h^+\right). \end{aligned} \tag{7d}$$

This interface velocity depends nonlinearly on the Reynolds number and the fiber length, as shown in Fig. 5 for a circular duct. Now, substitution of (7d) into (5c) results in the friction law for fiber-flocked surfaces:

$$\begin{aligned} \sqrt{\frac{8}{f}} \equiv u_m^+ &= (1 + \Lambda)\frac{\phi}{\kappa s} \\ &= \frac{1}{\kappa}\left\{\phi(\ln\xi + B_0) \right. \\ &\quad \left. + \frac{5\varepsilon\xi}{\omega(1 - \sigma)(5 - r_h)[1 + \xi\lambda N(\xi\lambda)]}\right\}. \end{aligned} \tag{8}$$

Since $\xi = \kappa R_H U_\tau/\nu = (1/2)\kappa Re/u_m^+ = (1/2)\kappa Re\sqrt{f}/8$, (8) is implicit for determining u_m^+ and f as functions of Re, similarly as the Prandtl friction law for smooth surfaces [4].

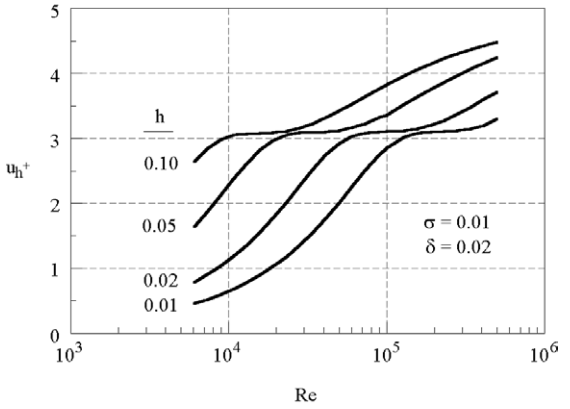

Fig. 5. Fiber-tip velocity variations.

The only unspecified parameter in (8) is the turbulence shift distance, $\lambda = h - y_t$, which must be determined by comparison with the experiment. For this purpose, flow-Δp tests were conducted with water-flow in two different tubes, flocked similarly with carbon fibers, for which $h = 0.0435$, $\delta = 0.022$, $\sigma = 0.08$ ($\varepsilon \approx 0.023$) [14]; the resulting friction factor data are shown in Fig. 6. By the adjustment $\lambda/h = 0.32$, there is fair agreement of (8) with these pressure-drop data at the higher Reynolds numbers, as seen, although there is considerable scatter in the low Reynolds number data.

The "relative roughness" of the experimental fibers is $h/2 = 0.022$; if this is used as a "sand-grain roughness", then the Moody curve shown is obtained [15]. It is seen that the flocked surface has slightly higher friction than sand grains, indicating a somewhat deeper penetration of the turbulence into the fiber region, which is consistent with the 32% turbulence penetration. This penetration means that enhanced heat transfer is expected since most heat transfer occurs near the fiber tips.

The friction results for a larger Reynolds number range is shown in Fig. 7 in comparison to the Prandtl smooth friction law. At the smallest turbulent Reynolds

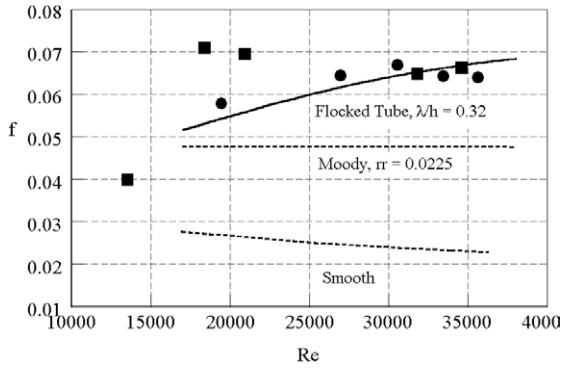

Fig. 6. Comparison of friction factor with data.

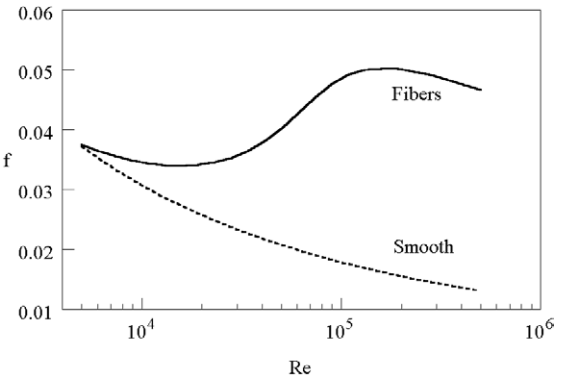

Fig. 7. Calculated friction factors.

number ($Re = 5000$), the smooth- and fiber-wall friction factors are about the same, but as Re increases, f_{fiber} increases before it decreases again, whereas f_{smooth} decreases uniformly. The undulating f_{fiber} behavior is typical of transitional roughness, and is the result of varying the roughness Reynolds number, $h^+ = hU_\tau/\nu$. Thus, as Re increases, the surface becomes progressively and dynamically more rough (i.e., the turbulence progresses farther into the fibers towards the limit, y_t).

3. Energy analysis

3.1. Derivation of energy equations

3.1.1. Central core region equations

In the fiber-free central core region of the duct, which ranges over $0 \leqslant R \leqslant R_H$ ($R_H \geqslant Z \geqslant 0$), the fully developed energy equation is

$$\frac{1}{R^n}\frac{\partial}{\partial R}\left(R^n \Gamma \frac{\partial T_c}{\partial R}\right) = \frac{U}{\alpha_g}\frac{\partial T_c}{\partial X}, \tag{9a}$$

or, with $R = R_H r = R_H(1-z)$, $\theta_c = (T_C - T_W)/(T_H - T_W)$

$$\frac{\partial}{\partial r}\left(r^n \frac{\Gamma}{\xi}\frac{\partial \theta_c}{\partial r}\right) = -\frac{S}{\xi} r^n u^+ = -\frac{S}{\xi} r^n \left(u_h^+ + \frac{v(w)}{\kappa s}\right), \tag{9b}$$

where the wall heat source parameter, S, is given by

$$S \equiv R^+ Pr \frac{\partial T_c/\partial X}{(T_W - T_H)/R_H} = R^+ Pr \frac{dT_{c,m}/dX}{(T_W - T_H)/R_H} = \frac{Nu\theta_m}{u_m^+},$$

where $u^+ = u_h^+ + v/\kappa s, \kappa s = U_\tau/V_c$, and where the core velocity, $v(w)$, is given by (5d): $v(w)/s = \ln(1+\xi w) + I_0(\xi w) - I_0(\xi\lambda) + (1+\lambda-w)[1 - Q_1(w)]$. Here, the second equality for S results from the constant wall-flux heat-transfer case ($q_w = \text{const.}$); for this case, S is a parameter to be determined from the solution (similar to the friction factor). When S is known, the overall Nusselt number is determined from $Nu = u_m^+ S/\theta_m$.

3.1.2. Fiber-region equations

We consider a surface flocked with fibers of height H and diameter d, as shown in Fig. 1. Above the fibers there is a flow which results in the axial velocity U_H and temperature T_H at $Y = H$. For a differential slice at distance Y, energy balances on the fiber (solid) and fluid (gas) control volumes yield the following equations [1]:

$$\frac{\partial^2 T_s}{\partial Y^2} - \frac{hP_s}{k_s A_s}(T_s - T_g) = 0, \tag{10a}$$

$$\frac{\partial}{\partial Y}\left(\Gamma \frac{\partial T_g}{\partial Y}\right) - \frac{hP_s}{k_g A_g}(T_g - T_s) = \frac{U}{\alpha_g}\frac{\partial T_g}{\partial X}, \tag{10b}$$

where h is the heat transfer coefficient between the fluid and fibers at distance Y from the wall. The laminar plus turbulent thermal diffusivity function is, in general

$$\Gamma = 1 + \frac{Pr}{Pr_t}\frac{\nu_t}{\nu} = 1 + p\xi M[z+\lambda]N[\xi(z+\lambda)], \tag{10c}$$

where $p = Pr/Pr_t \approx Pr/0.86$; however, in the fiber region as $z \to 0$, the velocity analysis shows that Γ becomes a constant, as follows:

$$\begin{aligned}\Gamma &= 1 + \frac{Pr}{Pr_t}\frac{\nu_t}{\nu} \to 1 + p\xi M(\lambda)N(\xi\lambda)\\ &= 1 + p\xi\lambda N(\xi\lambda).\end{aligned} \tag{10d}$$

Equations (10a) and (10b) are recognized as the thermal fin equation [16], and the one-dimensional convection equation [6]. Let nondimensional temperatures be defined by

$$\theta = \frac{T - T_W(X)}{T_H(X) - T_W(X)},$$

so that $\theta_g(X,0) = \theta_s(X,0) = 0$ and $\theta_g(X,H) = 1$. Then (10a) and (10b) appear as

$$\frac{\partial^2 \theta_s}{\partial y^2} - \frac{1}{\varepsilon_H^2}(\theta_s - \theta_g) = 0, \tag{11a}$$

$$\frac{\partial}{\partial y}\left(\Gamma \frac{\partial \theta_g}{\partial y}\right) - \frac{r_k}{\varepsilon_H^2}(\theta_g - \theta_s) = -Su^+, \tag{11b}$$

where the fiber heat transfer, ε_H, and conductivity ratio, r_k, parameters are

$$\varepsilon_H \equiv \frac{d}{2R_H\sqrt{Nu_d k_g/k_s}}, \quad r_k \equiv \frac{k_s}{k_g}\frac{\sigma}{1-\sigma}.$$

The complete solution of (11a)–(11c) requires the local fiber-diameter Nusselt number, $Nu_d = hd/k_g$, usually as a function of the local Reynolds number, $Re_d = \rho U d/\mu = u^+ d^+ \approx u_h^+ d^+$; that is, we shall find Nu_d to be important only near the fiber tips, so that $u^+ \approx u_h^+$ is an adequate approximation. Numerous correlations have been reported, depending on the Reynolds number range in question [1]; here we employ the Churchill and Bernstein correlation for $Re_d > 0.2/Pr$ [16,17]:

$$Nu_d = 0.3 + 0.62 Re_d^{1/2} Pr^{1/3}\frac{(1 + (Re_d/282\,000)^{5/8})^{4/5}}{(1 + (0.4/Pr)^{2/3})^{1/4}}. \tag{11c}$$

Since Γ is constant in the fiber region, let $\Omega^2 = (\Gamma + r_k)/\Gamma$, and $\psi = \theta/S$, then the fiber-region energy equations (11a) and (11b) become

$$\varepsilon_H^2\frac{\partial^2 \psi_s}{\partial y^2} - \Omega^2\frac{\Gamma}{\Gamma + r_k}(\psi_s - \psi_g) = 0, \tag{12a}$$

$$\varepsilon_H^2\frac{\partial^2 \psi_g}{\partial y^2} - \Omega^2\frac{r_k}{\Gamma + r_k}(\psi_g - \psi_s) = -\varepsilon_H^2 u^+/\Gamma. \tag{12b}$$

3.2. Solution of energy equations

3.2.1. Fiber-region solutions

The fiber-region thermal solutions are obtained first. Regardless of the value of Nu_d, (11a) and (11b) can be combined to yield

$$\begin{aligned}\frac{\partial^2}{\partial y^2}(\Gamma\theta_g + r_k\theta_s) &= -Su^+\\ &= -S\frac{u_h^+}{5}\left\{r_h - (5 - r_h)e^{-\omega(h-y)/\varepsilon}\right\}\end{aligned} \tag{13a}$$

with u^+ from (6c). Thus, the fluxes are related by

$$\begin{aligned}&\frac{\partial}{\partial y}(\Gamma\theta_g + r_k\theta_s) = -S\int u^+\,dy + C_1\\ &\text{with}\\ &\int u^+\,dy = \frac{u_h^+}{5}\left\{r_h y - (5 - r_h)(\varepsilon/\omega)e^{-\omega(h-y)/\varepsilon}\right\}.\end{aligned} \tag{13b}$$

At the wall, $q_w = (1-\sigma)q_{w,g} + \sigma q_{w,s}$, such that with the Fourier conduction this leads to the requirement

$$(1-\sigma)\left.\frac{\partial\theta_g}{\partial y}\right|_{y=0} + \sigma\frac{k_s}{k_g}\left.\frac{\partial\theta_s}{\partial y}\right|_{y=0} = \frac{1}{2}u_m^+ s = \frac{1}{2}Nu\theta_m,$$

where u_m^+ is the mean value of u^+ over the core; thus, in (13b), $C_1 = u_m^+ S/2(1-\sigma)$. A further integration of (13b) yields the relationship between the fiber-region temperatures:

$$\Gamma\theta_g + r_k\theta_s = \frac{1}{2}\left[\frac{u_m^+}{1-\sigma}y - \frac{u_h^+ r_h}{5}y^2 + O(\varepsilon^2)\right]S + C_2. \tag{13c}$$

Here $C_2 = 0$ because both nondimensional temperatures are zero at $y = 0$.

For the tip condition of the fibers, H is taken such that the usual fin extension is included and such that $[d\theta_s/dy]_{y=h} = 0$ [16]; therefore, (13b) yields the expression for Nu and S:

$$\frac{Nu\theta_m}{u_m^+} \equiv S = \frac{\Gamma[\partial\theta_g/\partial y]_{y=h}}{\gamma_H},$$
$$\gamma_H \equiv \frac{u_m^+/2}{1-\sigma} - \frac{u_h^+}{5}[r_h h - \varepsilon(5-r_h)/\omega] + \cdots. \tag{13d}$$

Now, substitution of (13c) into (12a) yields a single equation for integration:

$$\varepsilon_H^2 \frac{\partial^2\psi_s}{\partial y^2} - \Omega^2\psi_s = -\frac{\Omega^2}{2(\Gamma+r_k)}\left\{\frac{u_m^+}{1-\sigma}y - \frac{u_h^+ r_h}{5}y^2\right\}, \tag{14a}$$

where $\psi_s \equiv \theta_s/S$. Because $\varepsilon_H \ll 1$, (14a) is also a singular perturbation equation. Thus, the outer solution is

$$\psi_s^o = \frac{1}{2(\Gamma+r_k)}\left\{\frac{u_m^+}{1-\sigma}y - \frac{u_h^+ r_h}{5}y^2\right\}. \tag{14b}$$

Since this goes to 0 for $y = 0$, there is no thermal boundary layer at the wall. For the fiber-tip region we take $\eta_H = (h-y)/\varepsilon_H$; then the inner solution of (14a) is of the form $\exp(-\Omega\eta_H)$, and the outer plus inner solutions are

$$\psi_s = \frac{1}{2(\Gamma+r_k)}\left\{\frac{u_m^+}{1-\sigma}y - \frac{u_h^+ r_h}{5}y^2 + b_s e^{-\Omega(h-y)/\varepsilon_H}\right\} \tag{14c}$$

setting the slope of (14c) to zero at $y = h$, we have $b_s = -(\varepsilon_H/\Omega)[u_A^+/(1-\sigma) - 2hu_h^+ r_h/5]$. Therefore, the solution of (14c) gives the solid temperature as

$$\psi_s = \frac{1}{2(\Gamma+r_k)}\left\{\frac{u_m^+}{1-\sigma}y - \frac{u_h^+ r_h}{5}y^2 - \frac{\varepsilon_H}{\Omega}\left(\frac{u_m^+}{1-\sigma} - \frac{2}{5}hu_h^+ r_h\right)e^{-\Omega(h-y)/\varepsilon_H}\right\}, \tag{14d}$$

and with (13c) the fluid temperature is

$$\psi_g = \frac{1}{2(\Gamma+r_k)}\left\{\frac{u_m^+}{1-\sigma}y - \frac{u_h^+ r_h}{5}y^2 + \frac{\varepsilon_H r_k}{\Omega\Gamma}\left(\frac{u_m^+}{1-\sigma} - \frac{2}{5}hu_h^+ r_h\right)e^{-\Omega(h-y)/\varepsilon_H}\right\}. \tag{14e}$$

These temperatures are shown in Fig. 8 for several values of k_g/k_s and S, with θ_g as solid lines and the corresponding θ_s as dashed lines. All solid lines proceed to $\theta_g = 1$ as $y \to h$, and the slopes of θ_s go to zero, as required. The difference between (14e) and (14d) yields the lateral temperature potential that drives the heat transfer between the fluid and fibers:

$$\theta_g - \theta_s = \frac{\varepsilon_H S}{2\Omega\Gamma}\left(\frac{u_m^+}{1-\sigma} - \frac{2}{5}hu_h^+ r_h\right)e^{-\Omega(h-y)/\varepsilon_H}. \tag{15}$$

Thus, the lateral potential is exponentially small except near the fiber tips as $y \to h$; however, as the fiber conductivity is increased, the nonzero potential reaches further into the fiber region. These solutions are similar

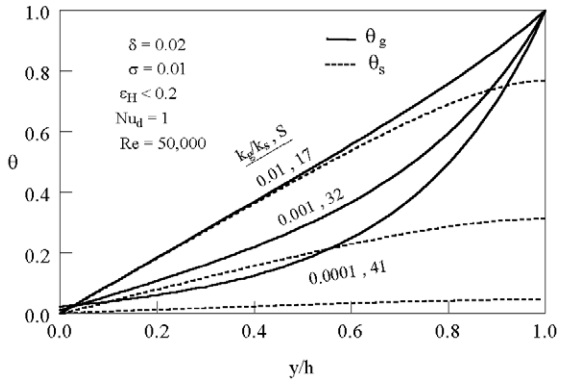

Fig. 8. Fiber-region temperature profiles.

to those for laminar flow [1], except that the factor S is here much larger.

Now, since $\psi_g(h) = 1/S$, we have from (14e)

$$\frac{2(\Gamma+r_k)}{S} = \frac{u_m^+}{1-\sigma}\left(h + \frac{\varepsilon_H r_k}{\Omega\Gamma}\right) - \frac{u_h^+ r_h}{5}\left(h^2 + 2\frac{\varepsilon_H r_k}{\Omega\Gamma}h\right) \approx \frac{u_m^+}{1-\sigma}\left(h + \frac{\varepsilon_H r_k}{\Omega\Gamma}\right). \tag{16}$$

In all of these solutions, Γ is the constant value for the fiber region given by (10d).

3.2.2. Central core region solutions

For the core thermal solution, let $\theta_c = \theta_{CL} - (S/\xi)G_0(w)$. Then (9b) results in

$$\frac{\partial}{\partial r}\left(r^n\frac{\Gamma}{\xi}\frac{\partial G_0}{\partial r}\right) = r^n u_h^+ + \frac{r^n}{\kappa}\{\ln(1+\xi w) + I_0(\xi w) - I_0(\xi\lambda) + r[1 - Q_1(w)]\}. \tag{17}$$

The first integral of (17) is therefore

$$\frac{\Gamma}{\xi}\frac{\partial G_0}{\partial r} = \left(\frac{1}{\xi} + pM(w)N(\xi w)\right)\frac{\partial G_0}{\partial r} = \frac{u_h^+ r}{n+1} + \frac{r^2}{(n+2)\kappa} + \frac{1}{\kappa r^n}\{K_1 + K_2 - K_3\}, \tag{18a}$$

where, for $\xi \gg 1$ and $\lambda \ll 1$,

$$K_1 = \int_0^r r^n \ln[1+\xi(1-r)]\,dr = \frac{1}{n+1}\{\ln(1+\xi) - (1-r^{n+1})\ln(1+\xi z) - r(1+r/2)^n\},$$

$$K_2 = \int_0^r r^n[I_0(\zeta) - I_0(\xi\lambda)]\,dr = \frac{1}{n+1}\left\{r^{n+1}\Delta I_0 - \int_0^r r^{n+1}\frac{dI_0}{d\zeta}\frac{d\zeta}{dr}\,dr\right\} = \frac{1}{n+1}\{J_0 - I_0(\zeta) + r^{n+1}[I_0(\zeta) - I_0(\xi\Gamma)]\} + O(1/\xi),$$

$$K_3 = \int_0^r r^{n+1} Q_1(w)\,\mathrm{d}r = \frac{1}{n+1}\left\{ r^{n+2} Q_1(w) - \int_0^r r^{n+1} \frac{\mathrm{d}(rQ_1)}{\mathrm{d}w}\frac{\mathrm{d}w}{\mathrm{d}r}\,\mathrm{d}r \right\} = \frac{r^{n+2}}{n+1}\{Q_1(w) - Q_{n+2}(w)\}.$$

For the second integral of (17), let $G_0 = [u_h^+/(n+1)]G_{0h} + [1/(n+1)\kappa]G_{0\kappa}$. Then, with zero slope at the centerline, the core-temperature first integrals are

$$\frac{\Gamma}{\xi}\frac{\partial G_0 h}{\partial r} = \left(\frac{1}{\xi} + pM(w)N(\xi w)\right)\frac{\partial G_0 h}{\partial r} = r, \tag{18b}$$

$$\frac{\Gamma}{\xi}\frac{\partial G_{0\kappa}}{\partial r} = \frac{[\ln(1+\xi) - (1-r^{n+1})\ln(1+\xi w) + J_0 - I_0(\zeta)]}{r^n} - (1+r/2)^n r^{n-1} + r\{I_0(\zeta) - I_0(\xi\lambda)\} - r^2\left\{Q_1 - Q_3 - \frac{n+1}{n+2}\right\}. \tag{18c}$$

For (18b) the outer and inner equations are

$$p\frac{w}{1+wP(w)}\frac{\partial G_{0h}^{\mathrm{o}}}{\partial w} = -(1-w), \tag{19a}$$

$$(1+p\zeta N(\zeta))\frac{\partial G_{0h}^{\mathrm{i}}}{\partial \varsigma} = -(1-\zeta/\xi) \approx -1. \tag{19b}$$

The solution of (19a), subject to $G_{0h}^{\mathrm{o}}(1) = 0$, is

$$G_{0h}^{\mathrm{o}} = \frac{1}{p}\{-\ln w + (1-w)(Q_1(w) - 1)\}, \tag{20a}$$

where Q_1 is given by (3c), and the solution of (19b) is

$$G_{0h}^{\mathrm{i}} = G_{0h}^{\mathrm{i}}(0) - \frac{1}{p}\ln(1+p\zeta) - I_1(\zeta). \tag{20b}$$

where I_1 is given by (4c). Then matching (20a) and (20b) we have the initial value

$$G_{0h}^{\mathrm{i}}(0) = \frac{1}{p}\{\ln(p\xi) + Q_1(0) - 1\} + J_1 \tag{20c}$$

with $J_1 = I_1(\infty)$; thus, the composite expansion is

$$G_{0h}^{\mathrm{c}} = \frac{1}{p}\left\{-\ln\left(\frac{1}{\xi p} + w\right) + (1-w)(Q_1(w) - 1)\right\} + J_1 - I_1(\xi w). \tag{20d}$$

For (18c) it is more convenient to use numerical integration. An example of both functions is shown in Fig. 9 for the circular duct ($n = 1$). Near the fiber tips ($r = 1$), these variables increase rapidly to their interface values, $G_{0h}(1)$ and $G_{0\kappa}(1)$. With the G_0-function thus determined, we then have the core temperature distribution

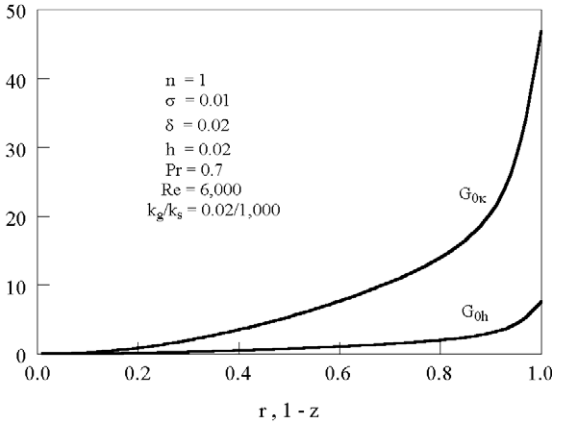

Fig. 9. Core-region temperature functions.

$$\theta_{\mathrm{c}}(r) = \theta_{\mathrm{CL}} - \frac{S}{\xi}G_0 = \theta_{\mathrm{CL}} - \frac{S}{\xi}\left(\frac{u_h^+}{n+1}G_{0h}(r) + \frac{1}{(n+1)\kappa}G_{0\kappa}(r)\right), \tag{21a}$$

and, since $\theta_{\mathrm{c}}(1) = 1$, the centerline temperature is

$$\theta_{\mathrm{CL}} = 1 + \frac{S}{\xi}\left(\frac{u_h^+}{n+1}G_{0h}(1) + \frac{1}{(n+1)\kappa}G_{0\kappa}(1)\right). \tag{21b}$$

3.3. Nusselt number results

To determine the Nusselt number, the mean bulk temperature is needed. This is obtained by a further numerical averaging integration of (21a) and (21b), thus forming the tip minus core-mean values, $\Delta G_{0h} = G_{0h}(1) - G_{0h,m}$ and $\Delta G_{0\kappa} = G_{0\kappa}(1) - G_{0\kappa,m}$. Then, the average core temperature is given by

$$\theta_{\mathrm{m}} = 1 + \frac{S}{\xi}\left(\frac{u_h^+}{n+1}\Delta G_{0h} + \frac{1}{(n+1)\kappa}\Delta G_{0\kappa}\right). \tag{22}$$

Because the fibers are short, and θ is small near the wall, (22) suffices for the overall bulk average.

In view of these considerations, the final expression for $Nu = u_m^+ S/\theta_{\mathrm{m}}$ is given by (23):

$$Nu = u_m^+ S \Big/ \left\{1 + \frac{S}{\xi(n+1)}\left(u_h^+\Delta G_{0h} + \frac{1}{\kappa}\Delta G_{0\kappa}\right)\right\}. \tag{23}$$

The results of computations with (23) are shown in Fig. 10, in comparison to the smooth-wall Gnielinski/Petukhov correlation [16]. For the curve labeled "A" the increase in *Nu* with *Re* follows the standard, smooth-surface behavior, but at higher *Re* values the fiber-surface results in greater *Nu* values by a factor of *two*. Although this degree of enhancement is somewhat larger than for some other types of surface augmentation [18,19], it is fairly typical in turbulent duct flow.

The fiber-surface heat transfer tends to increase with the solid packing fraction, σ, and fiber length ratio, h, as well as with a smaller slenderness ratio, δ; therefore, these parameters were changed to the values shown in Fig. 10 as curve "B". Now it is seen that, for high-conductivity fibers, a factor of *four* enhancement is possible. Such a degree of improvement is difficult to achieve with other types of surface augmentations. The above results are for gases with $Pr \approx 0.7$.

At conventional smooth and partially-rough walls, the Prandtl number primarily affects conduction across the viscous sublayer. By contrast, for fiber-flocked walls, Pr affects the turbulent diffusion of heat between the fibers, and thus the heat transfer all along the exposed fiber surfaces; since the fibers have a very large aspect ratio, a considerable amplification of the Pr effect may be expected.

The effect of the Prandtl number is shown in Fig. 11 where the computed curve is compared to smooth-wall correlations for liquid metals, and for gases and viscous liquids [6]; a representative fluid conductivity, k_g, varies linearly from 100 W/m K at $Pr = 0.01$ to 0.1 W/m K at $Pr = 100$, for illustration, and the solid conductivity is fixed at $k_s = 1000$ W/m K. Although the Nu_d correlation is extended below its experimental range, it is seen that there is uniform enhancement for small and moderate Prandtl numbers, and that for large Pr a very large enhancement is predicted with approximate first-power variation $Nu \sim Pr$.

The strong Pr variation can be seen in the limits of the analytical solutions: for $\xi \to \infty$, $Nu \to u_m^+ S$ in (23); thus from (16), and with $\Omega^2 \equiv (\Gamma + r_k)/\Gamma$,

$$Nu \to u_m^+ S \approx \frac{2(1-\sigma)(\Gamma + r_k)}{h + [(\varepsilon_H r_k)/(\Omega\Gamma)]} = \frac{2(1-\sigma)\Gamma^{1/2}(\Gamma + r_k)^{3/2}}{\varepsilon_H r_k + h\sqrt{\Gamma(\Gamma + r_k)}}.$$

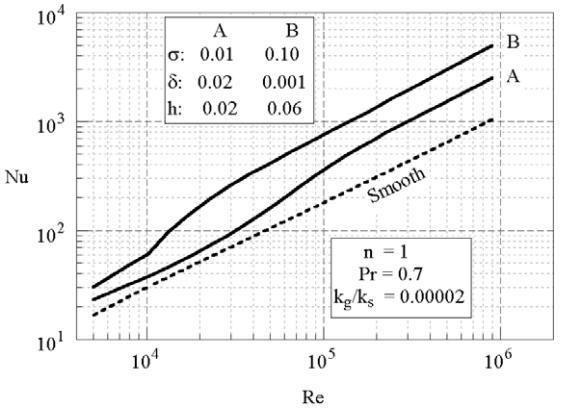

Fig. 10. Variation of Nusselt number with Reynolds number.

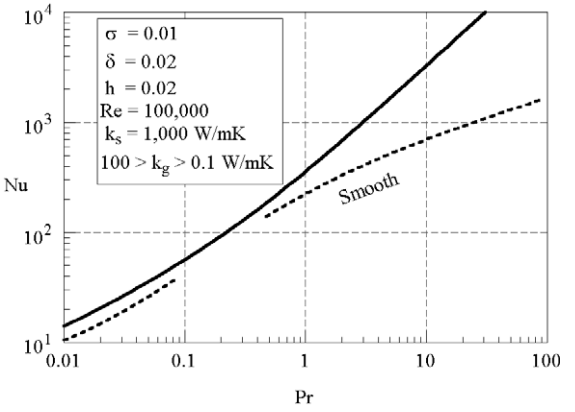

Fig. 11. Variation of Nusselt number with Prandtl number.

Since from (10d) $\Gamma \sim Pr$, it is seen that there is a strong effect of Pr on Nu for fiber-flocked surfaces. There is also some Pr effect through ε_H and Nu_d from (11a)–(11c). Hence, the results of the analysis show that fiber-flocked heat transfer surfaces may yield an order of magnitude enhancement for water and viscous liquids.

4. Conclusion

Using accepted turbulence modeling techniques and perturbation analysis, in conjunction with experimental fine-cylinder drag coefficients and Nusselt numbers, velocity and temperature profiles were determined for turbulent flow and heat transfer about the fibers at the duct surface as well as in the duct core. These profiles show large gradients near the tips of the fibers, which lead to large heat transfer enhancements. The results show that, for gases, a factor of four enhancement is possible with the fiber-flocked surfaces. Moreover, even greater order-of-magnitude enhancements are predicted for water and viscous liquids.

Acknowledgements

The present work was generously supported by a research gift from Energy Science Laboratories, to the University of California, San Diego.

References

[1] K.O. Lund, T.R. Knowles, Enhanced laminar-flow heat transfer at fiber-flocked surfaces, Int. J. Heat Mass Transfer 44 (2001) 1627–1636.

[2] A. Bejan, Theory of heat transfer from a surface covered with hair, J. Heat Transfer 112 (1990) 662–667.

[3] A.J. Fowler, A. Bejan, Forced convection from a surface covered with flexible fibers, Int. J. Heat Mass Transfer 38 (1995) 767–777.
[4] H. Schlichting, Boundary Layer Theory, McGraw-Hill, New York, 1968.
[5] F.M. White, Viscous Fluid Flow, McGraw-Hill, New York, 1974.
[6] W.M. Kays, M.E. Crawford, Convective Heat and Mass Transfer, second ed., McGraw-Hill, New York, 1980.
[7] P.-A. Krogstad, Modification of the Van Driest damping function to include the effects of surface roughness, AIAA J. 29 (6) (1991) 888–894.
[8] F.R. Menter, Two-equation eddy-viscosity turbulence models for engineering applications, AIAA J. 32 (8) (1994) 1598–1605.
[9] A. Hellsten, S. Laine, Extension of the k–ω–SST turbulence model for flows over rough surfaces, AIAA Paper No. AIAA-97–3577, 1997.
[10] K.O. Lund, W.B. Bush, Asymptotic analysis of plane turbulent Couette–Poiseuille flows, J. Fluid Mech. 96 (part 1) (1980) 81–104.
[11] K.O. Lund, Asymptotic analysis of turbulent flow for a rotating cylinder, in: K. Gersten (Ed.), Proceedings of the International Union of Theoretical and Applied Mechanics: Symposium on Asymptotic Methods for Turbulent Shear Flows at High Reynolds Numbers, Kluwer Academic Publishers, 1996, pp. 45–58.
[12] J.O. Hinze, in: Turbulence, McGraw-Hill, New York, 1959, p. 525.
[13] A.K.M.F. Hussain, W.C. Reynolds, Measurements in fully developed turbulent channel flow, J. Fluids Eng. 97 (1975) 568–580.
[14] M. Ahmadi, Personal communication, Energy Science Laboratories, San Diego, CA, 29 May 1999.
[15] L.F. Moody, Friction factors for pipe flow, Trans. ASME (November 1944) 671–684.
[16] F.P. Incropera, D.P. DeWitt, Fundamentals of Heat and Mass Transfer, fourth ed., Wiley, New York, 1996.
[17] S.W. Churchill, M. Bernstein, J. Heat Transfer 99 (1977) 300.
[18] J.Y. Yun, K.S. Lee, Investigation of heat transfer characteristics on various kinds of fin-and-tube heat exchangers with interrupted surfaces, Int. J. Heat Mass Transfer 42 (1999) 2375–2385.
[19] R. Karwa, S.C. Solanki, J.S. Saini, Heat transfer coefficient and friction factor correlations for the transitional flow regime in rib-roughened rectangular ducts, Int. J. Heat Mass Transfer 42 (1999) 1597–1615.